Journal of Materials Chemistry A

ROYAL SOCIETY OF CHEMISTRY

PAPER

View Article Online
View Journal | View Issue

Cite this: J. Mater. Chem. A, 2020, 8, 3651

A color-tunable fluorescent pillararene coordination polymer for efficient pollutant detection†

Xiang-Shuai Li,[ab] Yong-Fu Li,[a] Jia-Rui Wu,[a] Xin-Yue Lou,[a] Junyou Han,*[b] Jianchun Qin*[b] and Ying-Wei Yang *[ac]

Received 16th December 2019
Accepted 20th January 2020

DOI: 10.1039/c9ta13776a

rsc.li/materials-a

A dicarboxylatopillar[5]arene (DCP5)-based coordination polymer, namely DCP5-Eu_xTb_y, with color-tunable emission and capable of nitroaromatic pollutant detection, has been designed and fabricated *via* a typical metal–ligand coordination approach. Due to its rigid skeleton and electron-rich cavity, DCP5 plays an important role in this multi-color framework, not only as a linker but also as a blue-color fluorescence donor. Intriguingly, the fluorescent color of DCP5-Eu_xTb_y can be tuned from green to red simply by mediating the molar ratio of Eu^{3+} : Tb^{3+} in the functional system. More importantly, a white-color emitting system, that is, DCP5-Eu_1Tb_3, is discovered when the ratio of Eu^{3+} : Tb^{3+} is 1 : 3, and the white-light emissive DCP5-Eu_1Tb_3 exhibits good detection performance toward nitroaromatic pollutants in a wide application field. We envision that this work will open a new avenue for the exploration of synthetic macrocycle-based new materials in the construction of new fluorescent sensors and detectors for environmental sustainability and bio-related fields.

1 Introduction

A supramolecular toolbox containing several generations of synthetic macrocycles[1–6] has occupied a significant leading position in chemistry and materials science over the past few decades. Due to their tailored structures and tunable host–guest properties, supramolecular macrocycles have found applications in many chemical research areas.[7–11] Among various macrocyclic arenes, pillar[*n*]arenes (pillararenes, or pillarenes for short), the most representative ones that possess a rigid macrocyclic frame, π-electron rich cavity, and many possibilities of easy functionalization, have emerged as a new star in supramolecular chemistry and materials since the discovery by Ogoshi and co-workers in 2008;[12–18] however, their capabilities have still been far undervalued. Pillarenes with an inherent rigid skeleton can serve as natural bridges to construct novel framework materials; therefore a number of functional materials with pillarenes as core strut components have emerged, such as supramolecular organic frameworks (SOFs),[19,20] conjugated macrocycle polymers (CMPs),[21] and metal–organic frameworks (MOFs),[22] which have shown great potential in gas selective capture, organic pollutant detection, and heavy metal ion sensing and removal.[23–26] Apart from the rigid structure, it should be pointed out that, possessing electron-rich, large conjugated, and de-localized cavity, pillarenes may also be an excellent energy donor candidate to develop novel fluorescent materials, but their optical properties have always been ignored. Therefore, we are longing to design and construct a new type of pillarene-based fluorescent coordination polymer that is of high exploitability and research value in the field of organic–inorganic hybrid materials.

Coordination of metal ions and organic ligands has opened up a promising pathway to develop novel functional hybrid materials including coordination polymers (CPs) and/or MOFs.[27–34] Among various frameworks and polymers, new coordination ligands are always the key elements in determining their fascinating functions such as selective separation,[35,36] energy storage,[37,38] fluorescence,[39,40] and catalysis.[41,42] Therefore, exploration of new synthetic ligands with intrinsic functions is an effective route to the design and fabrication of novel functional materials and nanosystems.

On the other hand, nitroaromatic pollutants, which are composed of a benzene ring with several nitro and/or amino groups, have always been utilized as explosives and pesticides, and are seriously harmful to human health and environmental safety.[43] Importantly, this class of organic molecules is hard to detect, especially in biological systems, because of their

[a]State Key Laboratory of Inorganic Synthesis and Preparative Chemistry, International Joint Research Laboratory of Nano-Micro Architecture Chemistry (NMAC), College of Chemistry, Jilin University, 2699 Qianjin Street, Changchun 130012, P. R. China. E-mail: ywyang@jlu.edu.cn

[b]College of Plant Science, Jilin University, 5333 Xi'an Street, Changchun 130062, P. R. China. E-mail: hanjy@jlu.edu.cn; qinjc@jlu.edu.cn

[c]The State Key Laboratory of Refractories and Metallurgy, School of Chemistry and Chemical Engineering, Wuhan University of Science and Technology, Wuhan 430081, P. R. China

† Electronic supplementary information (ESI) available. See DOI: 10.1039/c9ta13776a

moderate vapor pressure and normal reactivity.[44] Thus, it is of great challenge and also in urgent need to develop portable and easy-achieving sensors for organic pollutant detection.[45] Among various fluorescent sensors, white-light emitting sensors are particular and popular due to their superior color fidelity and low color distortion.

Here we report on the design and synthesis of a novel color-tunable fluorescent pillarene coordination polymer (PCP), in which di-carboxylatopillar[5]arene (DCP5) is utilized as the coordination ligand and lanthanide metal ions, that is, europium (Eu^{3+}) and terbium (Tb^{3+}), as coordination central ions (Fig. 1). The obtained PCP is abbreviated as DCP5-Eu_xTb_y, where $x:y$ represents the molar ratio of $Eu^{3+}:Tb^{3+}$ in the composite material. Benefiting from its inherent blue fluorescence and electron-rich structure, the coordination ligand DCP5 dominantly contributes to the blue emission of DCP5-Eu_1Tb_3 and serves as an ideal energy donor for lanthanide metal ions. Interestingly, the red-color fluorescence intensity of this system is dominated by Eu^{3+} concentration, and Tb^{3+} concentration determines its green luminescence intensity; therefore the combined fluorescence color of DCP5-Eu_xTb_y could be tuned from red to green by simply changing the ratio of $x:y$. Notably, when $x:y$ is mediated to be 1 : 3, the fabricated DCP5-Eu_1Tb_3 exhibits intriguing white light emission (0.31 and 0.31) at 340 nm light excitation, offering its extraordinary ability in the detection of nitroaromatic pollutants with high sensitivity. The reported macrocycle-based sensors in the literature usually emit single color luminescence thus limiting their applications (Table S1, ESI†). In the current work, our solid materials can be applied under various conditions, representing the first example of color-tunable pillarene-based solid material as the efficient sensor, and more importantly, white-color emission can also be achieved. Considering its practical application value, this PCP has been further applied in biological systems including zebrafish, Limnodrilus, and also vegetables, and our experimental results reveal that this newly developed DCP5-Eu_1Tb_3 material possesses great potential in the application of pollutant detection both *in vitro* and *in vivo*.

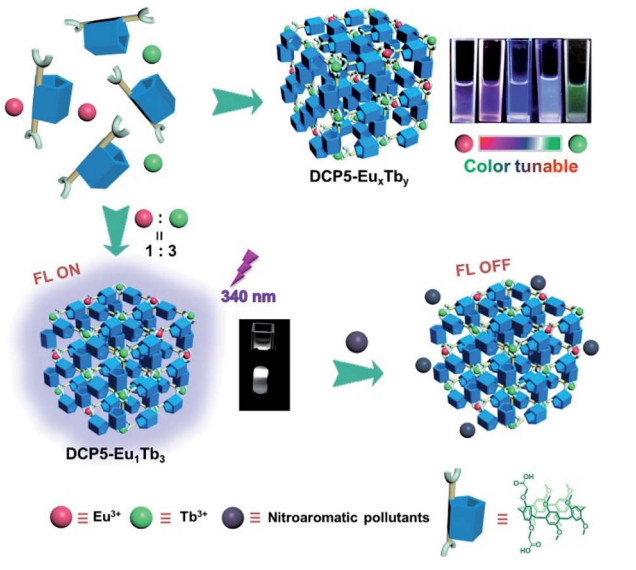

Fig. 1 Schematic illustration of the construction of the color-tunable pillarene coordination polymer (PCP), *i.e.*, DCP5-Eu_xTb_y, simply by tuning the molar ratio of Eu^{3+} and Tb^{3+} in the system and the fluorescence ON/OFF sensing of nitroaromatic pollutants by a typical PCP, *i.e.*, DCP5-Eu_1Tb_3.

2 Experimental section

2.1 Preparation of DCP5-Eu_xTb_y

DCP5-Eu_xTb_y was synthesized according to a typical solvent-thermal method; $EuCl_3 \cdot 6H_2O$ and $TbCl_3 \cdot 6H_2O$ with molar ratios of 1 : 0 (0.05 mmol : 0 mmol), 3 : 1 (0.0375 mmol : 0.0125 mmol), 1 : 1 (0.025 mmol : 0.025 mmol), 1 : 3 (0.0125 mmol : 0.0375 mmol), and 0 : 1 (0 mmol : 0.05 mmol) were added in five groups to Teflon reactors containing $AcONa \cdot 3H_2O$ (13.6 mg, 0.1 mmol) and DMF (10 mL), respectively. After this, DCP5 (44 mg, 0.05 mmol) was added to every reactor and subjected to ultrasound treatment for thorough dispersion. The reactors were kept at 150 °C for 24 h to give DCP5-Eu, DCP5-Eu_3Tb_1, DCP5-Eu_1Tb_1, DCP5-Eu_1Tb_3, and DCP5-Tb, respectively. Fourier transform infrared (FT-IR) spectroscopy, X-ray photoelectron spectroscopy (XPS), ^1H NMR spectroscopy, and energy-dispersive X-ray (EDX) spectroscopy were used to prove the successful coordination of DCP5 and lanthanide ions.

2.2 Detection of aromatic pollutants in zebrafish and Limnodrilus

At first, zebrafish and Limnodrilus were cultured in water that contained 0.3 mg mL^{-1} DCP5-Eu_1Tb_3 for 3 h and the fluorescence signals were observed in their bodies using a fluorescence microscope. Afterward, during the quenching process, these DCP5-Eu_1Tb_3 treated zebrafish and Limnodrilus were transferred into different concentrations of NB and 2-NA solutions for another 3 h. The pollutant treated animals and insects were observed using a fluorescence microscope to demonstrate the fluorescence intensity changes.

2.3 Extraction of cabbage tissues

Cabbage seeds were disinfected with 5% (m/m) $KMnO_4$ solution for 10 min, and water washed to remove the residual $KMnO_4$. Subsequently, these seeds were sown on filter paper, and deionized water and pollutant solutions were added to culture them. After culturing for five days, the cabbages were collected and ethanol was used to extract the organic compounds in the plant body by thoroughly grinding 3 times. The solution was concentrated for further detection.

3 Results and discussion

3.1 Rational design concept for the color-tunable fluorescent PCP

Bearing in mind the rigid cavity and large π-delocalized structure of pillarene,[46–48] a di-carboxylatopillar[5]arene derivative was prepared (Fig. S1–S6, ESI†) to perform the roles of both the strut and blue emission fluorophore in the PCP system.

Meanwhile, lanthanide ions (Eu^{3+} and Tb^{3+}) that contribute to red and green fluorescence were co-doped into the system as the coordination nodes to give a tri-color emitting PCP. The luminescence of DCP5-Eu_xTb_y exhibits an excitation wavelength-dependent behaviour; and at first, DCP5-Eu_1Tb_1 with a 1 : 1 molar ratio of Eu^{3+} : Tb^{3+} was fabricated to seek the optimal excitation wavelength. The excitation spectra of DCP5-Eu_1Tb_1 monitored at emission wavelengths of 546 nm and 619 nm (corresponding to Tb^{3+} and Eu^{3+}, the emission spectra of free Tb^{3+} and Eu^{3+} are shown in Fig. S7A and B, ESI†) show broad bands at 250–400 nm that could be attributed to the absorbance of DCP5 and f–f transitions of Eu^{3+} and Tb^{3+}, demonstrating the presence of energy transfer from the DCP5 ligand to central lanthanide ions (Fig. S8–S10, ESI†).[49,50] As illustrated in the fluorescence spectra (Fig. S11 and Table S2, ESI†), three main peaks at 430 nm, 546 nm, and 619 nm dominating blue, green, and red color emission, which are originated from DCP5 (Fig. S12, ESI†), $^5D_4 \rightarrow {}^7F_5$ transition of Tb^{3+}, and $^5D_0 \rightarrow {}^7F_2$ transition of Eu^{3+}, respectively, change continuously upon modulating the excitation wavelength from 300 nm to 380 nm thus leading to different emission colours of the system. This is due to the different energy transfer efficiencies from DCP5 to Eu^{3+} and Tb^{3+} at different excitations (Fig. S13, ESI†).[51–53] Notably, when excited at 340 nm, the luminescence color of DCP5-Eu_1Tb_1 is near to white-light (Fig. S7B, ESI†) with a CIE coordinate of (0.32, 0.27). On the basis of these results, we further tested and improved the quality and purity of the white-light emission of DCP5-Eu_xTb_y by modulating the molar ratio of Eu^{3+} : Tb^{3+} at an excitation of 340 nm.

DCP5 is crucial to perform as an energy donor for lanthanide ions. Upon gradual titration of Eu^{3+} and Tb^{3+} into DCP5 solution, the intensity of the peak at 430 nm assigned to DCP5 decreased and the intensity of the characteristic peaks of Eu^{3+} and Tb^{3+} were gradually enhanced (Fig. S14, ESI†), demonstrating the energy transfer processes from DCP5 to Eu^{3+} and Tb^{3+}. In the tri-color emission system, the combined fluorescence color of DCP5-Eu_xTb_y can be well controlled by simply changing the molar ratio of Eu^{3+} : Tb^{3+}. As in Fig. 2A, the fluorescence peaks that represent different colours changed continuously upon varying the constituent of lanthanide ions in DCP5-Eu_xTb_y. Subsequently, the fluorescence color of the obtained DCP5-Eu, DCP5-Eu_3Tb_1, DCP5-Eu_1Tb_1, DCP5-Eu_1Tb_3, and DCP5-Tb was distributed from amaranth to green as exhibited in the CIE coordinate (Fig. 2B and Table S3, ESI†) and the digital photos (Fig. 2C). Interestingly, a white-light emitting PCP abbreviated as DCP5-Eu_1Tb_3 was obtained when the Eu^{3+} : Tb^{3+} ratio was tuned to be 1 : 3 (Fig. 2D). In the following step, fluorescence lifetimes were measured to confirm the constituent of the DCP5-Eu_1Tb_3. The decay curve of DCP5 follows a double exponential decay, giving a fluorescence lifetime of $\tau = 5.39$ ns (Fig. S15, ESI†). As for DCP5-Eu_1Tb_3, a fluorescence lifetime of $\tau = 4.68$ ns measured at an emission wavelength of 430 nm is attributed to the contribution of DCP5 (Fig. S16A†), and in addition, lifetimes characterized at emission wavelengths of 546 nm and 619 nm were calculated to be $\tau = 0.90$ ms and $\tau = 0.78$ ms, respectively, indicating the existence of Eu^{3+} and Tb^{3+} in the material (Fig. S16B, C and Table S4, ESI†).

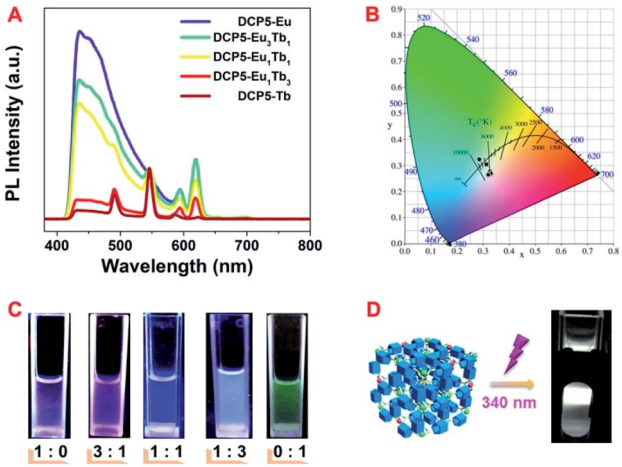

Fig. 2 (A) Fluorescence spectra of DCP5-Eu, DCP5-Eu_3Tb_1, DCP5-Eu_1Tb_1, DCP5-Eu_1Tb_3, and DCP5-Tb and (B) their corresponding CIE coordinates at 340 nm excitation. (C) Digital photos of DCP5-Eu_xTb_y with different x : y molar ratios of 1 : 0, 3 : 1, 1 : 1, 1 : 3, and 0 : 1 (from left to right) at 254 nm of UV irradiation. (D) Digital photo of DCP5-Eu_1Tb_3 excited by 340 nm light. [DCP5-Eu_1Tb_3] = 0.2 mg mL^{-1}, solvent: DMF, slit width: ex 10 nm, em 10 nm.

To examine the superiority and efficacy of DCP5 in this PCP system, we synthesized a control coordination ligand, 1,4-phenylenedioxydiacetic acid (PDDA), which shares the same terminal structure with DCP5 but without the macrocyclic cavity, to prepare a control polymer, namely PDDA-Eu_1Tb_3, according to the same synthetic method (Fig. S17–S19, ESI†). In the photoluminescence study of PDDA-Eu_1Tb_3, the blue emission peak of PDDA located at 447 nm shows extremely high intensity; however, peaks of lanthanide ions at 546 nm and 619 nm corresponding to green and red emission, respectively, are of very low intensity (Fig. S20A, ESI†). As a result, the fabricated PDDA-Eu_1Tb_3 only emits blue fluorescence and the CIE coordinate (0.17, 0.14) of the composite is located at blue color area (Fig. S20B†). This is due to the limited energy transfer efficiency from PDDA to lanthanide ions. In Fig. S21A, ESI,† no energy transfer from PDDA to Tb^{3+} was observed since the fluorescence intensity of PDDA (Fig. S22, ESI†) was retained upon continuous addition of Tb^{3+}, and meanwhile the energy transfer efficiency from PDDA to Eu^{3+} is extremely low (Fig. S21B, ESI†), only very weak characteristic peaks of Eu^{3+} emerged upon decreasing the fluorescence of PDDA. This sharp contrast in fluorescence behaviour between DCP5-Eu_1Tb_3 and PDDA-Eu_1Tb_3 implies that DCP5 plays an irreplaceable role in this tri-color emission system. The large conjugated structure of DCP5 can significantly contribute to the match between the lowest triplet state of the ligand and the first excited state of the lanthanide to enable the effective sensitization of Eu^{3+} and Tb^{3+}.[54,55]

3.2 Structural characterization

The formation of DCP5-Eu_1Tb_3 was further confirmed by FT-IR spectroscopy and XPS. As shown in Fig. 3A, the peak at 1719 cm^{-1} corresponding to the C=O stretching vibration of

carboxylic groups of DCP5 disappeared, indicating that the carboxylic acid groups were deprotonated due to the coordination of DCP5 and lanthanide ions.[56,57] The typical wide range XPS spectra (Fig. 3B) of DCP5 and DCP5-Eu_1Tb_3 showed C 1s and O 1s peaks, and the presence of the Tb 4d peak at 151.5 eV in XPS of DCP5-Eu_1Tb_3 confirmed the successful incorporation of lanthanide ions in the material.[58] In the O 1s spectra (Fig. 3C), both DCP5 and DCP5-Eu_1Tb_3 have two O 1s peaks positioned at 531.8 and 533.1 eV, in which the peaks at 531.8 eV can be assigned to the OH of DCP5 and the peaks at 533.1 eV can be attributed to the COO^- of DCP5 and the adsorbed H_2O.[44] After the coordination of DCP5 with lanthanide ions, the decreased peak at 531.8 eV demonstrated the successful coordination of the carboxyl group of DCP5 and lanthanide ions to result in a coordination polymer of DCP5-Eu_1Tb_3.[59] NMR titration experiments were further carried out, where the signals of protons H_{a1} shifted downfield and gradually became broad with the increased concentration of Eu^{3+} and Tb^{3+}. These pieces of evidence suggest that DCP5 and lanthanide ions were indeed in operation and coordinated into the polymers (Fig. S23 and S24, ESI†).[60]

Scanning electron microscopy (SEM) (Fig. 3D) and transmission electron microscopy (TEM) images (Fig. S25A, ESI†) illustrate the regular bulky morphology of the DCP5-Eu_1Tb_3 material. Upon comparison of the TEM images of free DCP5 showing amorphous structures (Fig. S25B, ESI†) with this regular DCP5-Eu_1Tb_3, we can easily find that the coordination polymer was successfully prepared. The type III N_2 adsorption–desorption isotherm indicates its nonporous nature (Fig. S26, ESI†). Besides, the EDX spectroscopy results show that Eu and Tb elements distribute uniformly in the bulk, demonstrating that both elements were incorporated into the composites (Fig. S27, ESI†). The molar ratio of Eu^{3+} : Tb^{3+} in DCP5-Eu_1Tb_3 calculated from EDX and inductively coupled plasma-atomic emission spectrometry (ICP) was 1 : 1.99 and 1 : 1.66, respectively (Table S5 and S6, ESI†), also suggesting that both Eu^{3+} and Tb^{3+} were successfully incorporated into the material framework with our expected ratio. As in the X-ray diffraction (XRD) patterns, the prepared polymer exhibits different regular peaks compared to DCP5, suggesting its good crystal phases and successful preparation (Fig. S28, ESI†). The thermal stability was evaluated according to thermogravimetric analysis (TGA); coordination ligands began to decompose at ~270 °C and the weight ratio of DCP5 in the composite was calculated to be ~65.7% (Fig. S29, ESI†). The successful formation of DCP5-Eu_1Tb_3 was further characterized using solid-state CP-MAS ^{13}C NMR spectroscopy (Fig. S30, ESI†). The peak at 30.5 ppm was assigned to the aliphatic methylene bridge ($-CH_2-$) of the DCP5 macrocycle, and the peak at 55.5 ppm was assigned to the methoxy moiety ($-OCH_3$) of DCP5. The peaks at 112.7, 128.8, and 150.7 ppm belong to the carbons of phenyl rings. In addition, SEM images of DCP5-Eu, DCP5-Eu_3Tb_1, DCP5-Eu_1Tb_1, and DCP5-Tb (Fig. S31, ESI†) show that these composites have bulky morphologies similar to those of DCP5-Eu_1Tb_3, and both XRD patterns (Fig. S32, ESI†) and FT-IR spectra (Fig. S33, ESI†) of the four PCPs show nearly identical peaks in comparison with DCP5-Eu_1Tb_3. These pieces of evidence clearly demonstrated that Eu^{3+} and Tb^{3+} were incorporated into the framework in a co-doping way that the structure of the PCP will not be affected by changing the molar ratio of Eu^{3+} : Tb^{3+}. On the other hand, the FT-IR results (Fig. S34, ESI†) demonstrated the successful preparation of the control polymer PDDA-Eu_1Tb_3, and the SEM image and XRD pattern illustrated its bloom-like shape and highly crystalline nature (Fig. S35 and S36, ESI†).

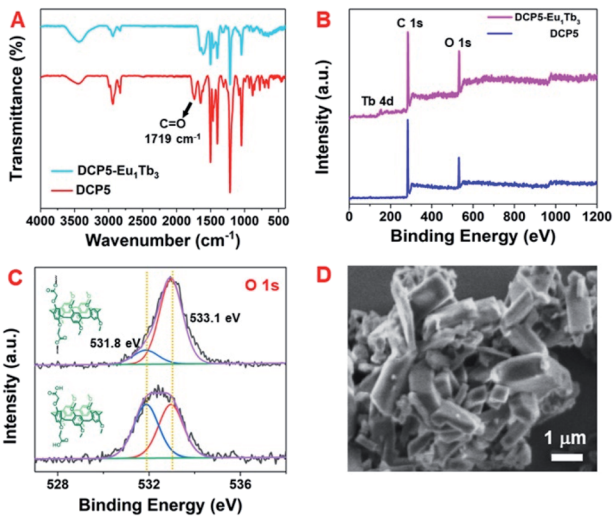

Fig. 3 (A) Fourier transform infrared (FT-IR) spectra of DCP5 and DCP5-Eu_1Tb_3. (B) Wide range and (C) O 1s regions of X-ray photoelectron spectroscopy (XPS) of DCP5 and DCP5-Eu_1Tb_3. (D) SEM image of DCP5-Eu_1Tb_3.

3.3 Nitroaromatic pollutant detection

Aromatic nitro compounds have been widely applied in the society as explosive and/or pesticide intermediates, greatly threatening human security and environmental safety. Thus, it is of great importance to develop some facile and highly efficient approaches for the detection of these organic pollutant residues. White light sensors have great practical values since they can ensure that the surroundings display their original colour. The studies of pollutant detection using our PCP materials were performed at an excitation of 340 nm under ambient environments. As in Fig. 4A–C and S37–S39, ESI,† white-light emissive DCP5-Eu_1Tb_3 showed quite efficient fluorescence quenching in response to nitrobenzene (NB), 2-nitrophenylamine (2-NA), and trinitrophenol (TNP). Upon titration of the analytes into DCP5-Eu_1Tb_3 dispersion, the quenching efficiencies of fluorescence reach 87.2%, 96.4%, and 91.7% as induced by NB, 2-NA, and TNP, respectively. The concentration of analytes also shows a good linear relationship against DCP5-Eu_1Tb_3 fluorescence intensity, indicating the promising potential of DCP5-Eu_1Tb_3 in real-time detection. The limit of detection (LOD) values for NB, 2-NA, and TNP are calculated in Fig. S40–S42, ESI,† both lower concentration (0.05 mg mL^{-1}) and higher concentration (1 mg mL^{-1}) of DCP5-Eu_1Tb_3 possess similar LOD values (73.4 μM and 65 μM, respectively) for NB detection, demonstrating that there is negligible concentration

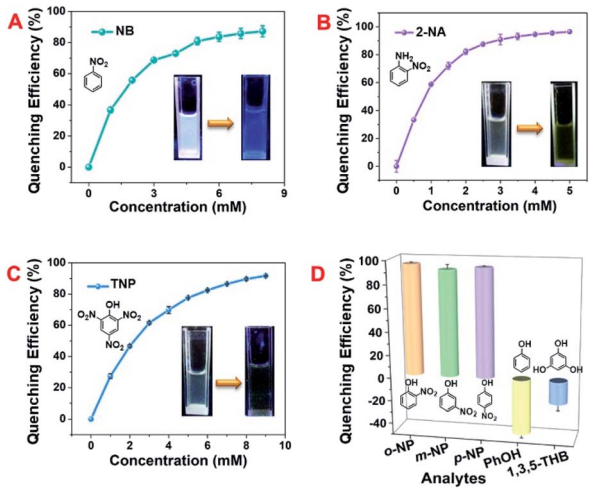

Fig. 4 Fluorescence quenching plots of DCP5-Eu_1Tb_3 upon addition of (A) nitrobenzene (NB), (B) 2-nitrophenylamine (2-NA), and (C) trinitrophenol (TNP). (D) Fluorescence quenching percentage of DCP5-Eu_1Tb_3 induced by different analytes of 10 mM. Solvent: DMF, λ_{ex}: 340 nm, slit width: ex 10 nm, em 10 nm.

restriction for DCP5-Eu_1Tb_3 application, and the LOD of DCP5-Eu_1Tb_3 for the detection of 2-NA and TNP is 83 μM and 51.6 μM, respectively. The quenching mechanism lies in the donor–acceptor electron transfer process, in which nitroaromatics stack with DCP5-Eu_1Tb_3 closely and electrons can be easily transferred from electron-rich DCP5-Eu_1Tb_3 to electron-withdrawing analytes, resulting in fluorescence quenching.[45,61] The electron transfer process can be demonstrated by the reduction potential. The lowest unoccupied molecular orbitals of NB, 2-NA, and TNP are low-lying and have reduction potentials (−1.53 V, −1.42 V, and −1.56 V) more positive than those of DCP5-Eu_1Tb_3 (−1.63 V, Fig. S43, ESI†); therefore, they can easily get electrons from the conduction band of DCP5-Eu_1Tb_3; meanwhile, the emission peak of DCP5-Eu_1Tb_3 showed an obvious bathochromic shift upon interaction with 2-NA and TNP, which could also strongly demonstrate the electron transfer process in accordance with the literature report (Fig. S38 and S39, ESI†).[62]

Several other analytes were subsequently measured to support this claim. As in Fig. 4D, electron-deficient *o*-nitrophenol, *m*-nitrophenol, and *p*-nitrophenol possessing a nitro group showed effective quenching effects towards DCP5-Eu_1Tb_3. However, when the analytes were changed to electron rich –OH groups containing phenol (PhOH) and 1,3,5-trihydroxyphenol (1,3,5-THB), the opposite effect, that is, fluorescence enhancement, was observed due to the electron-donating nature. This control experiment also demonstrates the good selectivity of DCP5-Eu_1Tb_3 for the detection of nitroaromatic pollutants. Besides, the other groups of materials (DCP5-Eu, DCP5-Eu_3Tb_1, DCP5-Eu_1Tb_1 and DCP5-Tb) were prepared according to the same method of DCP5-Eu_1Tb_3 and they have nearly the same structure; therefore they could also efficiently detect nitro-aromatic pollutants. For example, both DCP5-Eu and DCP5-Tb display good NB detecting ability (Fig. S44 and S45, ESI†).

3.4 Practical applications

Possessing advantages of excellent optical transparency, and a highly similar biological structure and physiological function to mammals, the zebrafish was thus utilized to evaluate the *in vivo* pollutant detection ability of the DCP5-Eu_1Tb_3 material. Excitingly, after zebrafish at the age of 6 dpf (days post fertilization) were incubated with DCP5-Eu_1Tb_3 for 3 h, the absorbed materials showed strong blue fluorescence in their bodies which is mainly distributed in the yolk mac (Fig. 5). Then, external pollutant solutions of 0.2 mM NB and 0.1 mM 2-NA were employed to culture these treated zebrafish separately. An obvious quenching phenomenon was observed in response to these pollutants even in living biological systems. The reason that DCP5-Eu_1Tb_3 exhibits white-color emission when dispersed in DMF solution yet shows blue fluorescence in the zebrafish body can be attributed to the solvent effect that the DMF solvent as the guest molecule in the DCP5-Eu_1Tb_3 channels was replaced by water molecules, and solvent molecules with different polarities in the materials' framework show various influences on the energy transfer process between DCP5 and metal ions, thus leading to different final fluorescence colors.[63,64]

For further validation, DCP5-Eu_1Tb_3 was dispersed in deionized water to evaluate its fluorescence spectra, and as in Fig. S46, ESI,† peaks of lanthanide ions turned negligible, but the blue emission peak of DCP5 was extremely high. As a result, DCP5-Eu_1Tb_3 finally emitted blue-color fluorescence which is in accordance with the former phenomenon in the zebrafish body (Fig. S46A and B, ESI†); besides, the CIE coordinate and digital photo also reveal its blue color emission in water (Fig. S46C and D, ESI†). Limnodrilus, which always lives in polluted water and serves as food for various fishes, possibly carries pollution in their body and further threaten the health of humans through

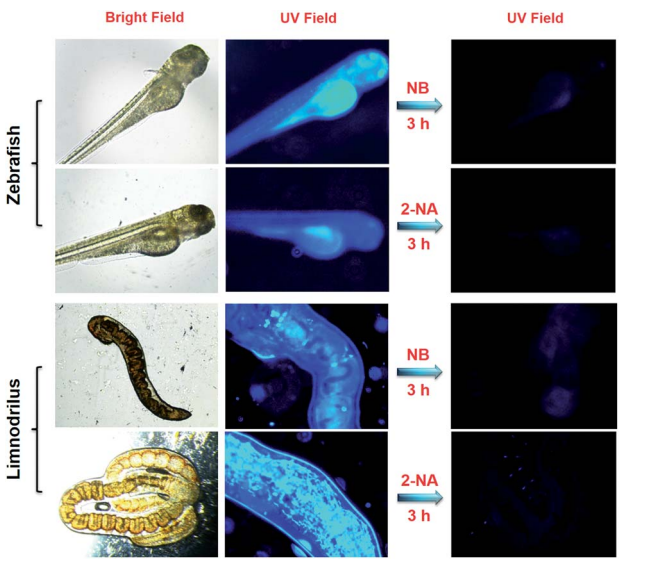

Fig. 5 Fluorescence microscopy images of zebrafish and Limnodrilus treated with DCP5-Eu_1Tb_3 (0.3 mg mL^{-1}) for 3 h and the corresponding images after being treated with NB (0.2 mM) and 2-NA (0.1 mM), respectively, for another 3 h (all *in vivo* experiments were carried out in water).

the food chain; therefore, DCP5-Eu_1Tb_3 was also applied in Limnodrilus. Excitingly, strong emission could be observed after these insects were cultured with DCP5-Eu_1Tb_3 and the fluorescence signal in the insects' bodies could be efficiently quenched by NB and 2-NA (Fig. 5). Given the favourable sensing results, DCP5-Eu_1Tb_3 can serve as a good candidate to monitor the nitroaromatic pollutants no matter *in vitro* or *in vivo*.

Food security is greatly bothering human health and safety, and plants and vegetables are imperative food sources in human daily life. In this work, cabbages were utilized as vegetable models to examine the application possibility of DCP5-Eu_1Tb_3 in agricultural fields. Cabbage seeds were sown in deionized water (control group) or pollutant solution (1 mM NB and 0.2 mM 2-NA in deionized water), respectively, and cultivated for five days to obtain polluted or unpolluted cabbages for further detection (Fig. S47, ESI†). As revealed from the digital photos, cabbages with NB and 2-NA groups were far shorter in size than the control group (Fig. 6A–C, and S48, ESI†), demonstrating the harmfulness of these pollutants on plants, and HR-MS spectroscopy was utilized to confirm that these pollutants were absorbed into plant bodies (Fig. S49 and S50, ESI†). The cabbage tissue extracts (CE) of the three groups were subsequently collected and titrated into DCP5-Eu_1Tb_3 solution to observe the following phenomena. Different from the control group (DCP5Eu_1Tb_3-CE-control) that exerted no obvious influence on the fluorescence of original solution, the fluorescence of DCP5-Eu_1Tb_3 treated with the extract of cabbages from NB and 2-NA groups (denoted as DCP5-Eu_1Tb_3-CE-NB and DCP5-Eu_1Tb_3-CE-2-NA) was largely quenched (Fig. 6D–F). These results fully affirmed the value of this novel DCP5-Eu_1Tb_3 material in agricultural applications.

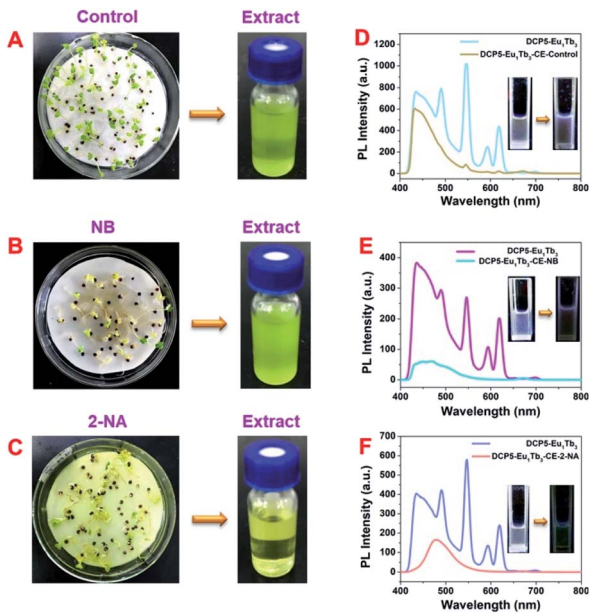

Fig. 6 Digital photos of cabbages (left) cultivated under (A) deionized water, (B) 1 mM NB water solution, and (C) 0.2 mM 2-NA water solution, respectively, and their tissue extract solution (right). Fluorescence spectra of DCP5-Eu_1Tb_3 before and after addition of cabbage extract: (D) control, (E) NB, and (F) 2-NA groups. The insets show their corresponding digital images. [DCP5-Eu_1Tb_3] = 0.2 mg mL^{-1}, solvent: DMF, λ_{ex}: 340 nm, slit width: ex 10 nm, em 10 nm.

4 Conclusions

In summary, we have demonstrated a new strategy to incorporate DCP5 supramolecular macrocycles into a lanthanide coordination polymer, resulting in an intriguing tri-color fluorescent PCP. Importantly, the combined emission color of DCP5-Eu_xTb_y can be well tuned from red to green by simply changing the molar ratio of Eu^{3+} : Tb^{3+}. In particular, the first type of white-color emitting pillarene-based PCP, that is, DCP5-Eu_1Tb_3, was obtained when Eu^{3+} : Tb^{3+} was adjusted to 1 : 3. Furthermore, this novel white-color fluorescent DCP5-Eu_1Tb_3 could selectively detect nitroaromatic pollutants through an electron transfer mechanism and exhibited remarkable potential in a wide range of biological platforms including fishes, insects, and vegetables due to its good optical properties. Therefore, we strongly believe that this type of newly designed fluorescent PCP will provide new insights for exploring the potential of macrocyclic arenes and play an important role in detecting and preventing pollutants.

Conflicts of interest

There are no conflicts to declare.

Acknowledgements

We thank the National Natural Science Foundation of China (51673084) and acknowledge the Jilin Province-University Cooperative Construction Project – Special Funds for New Materials (SXGJSF2017-3) and the Jilin University Talents Cultivation Program for financial support.

Notes and references

1 J.-M. Lehn, *Science*, 1985, **227**, 849–856.
2 S. Peacock, D. Walba, F. Geata, R. Helgeson and D. Cram, *J. Am. Chem. Soc.*, 1980, **102**, 2043–2052.
3 A. Harada, A. Hashidzume, H. Yamaguchi and Y. Takashima, *Chem. Rev.*, 2009, **109**, 5974–6023.
4 H. J. Kim, M. H. Lee, L. Mutihac, J. Vicens and J. S. Kim, *Chem. Soc. Rev.*, 2012, **41**, 1173–1190.
5 W. A. Freeman, W. L. Mock and N. Y. Shih, *J. Am. Chem. Soc.*, 1981, **103**, 7367–7368.
6 F. Diederich, *Angew. Chem., Int. Ed.*, 1988, **27**, 362.
7 S. Dong, B. Zheng, F. Wang and F. Huang, *Acc. Chem. Res.*, 2014, **47**, 1982–1994.
8 J. Zhou, G. Yu and F. Huang, *Chem. Soc. Rev.*, 2017, **46**, 7021–7053.
9 X. Hou, C. Ke and J. F. Stoddart, *Chem. Soc. Rev.*, 2016, **45**, 3766–3780.
10 Z. C. Liu, S. K. M. Nalluri and J. F. Stoddart, *Chem. Soc. Rev.*, 2017, **46**, 2459–2478.
11 K. Jie, Y. Zhou, E. Li and F. Huang, *Acc. Chem. Res.*, 2018, **51**, 2064–2072.

12 N. Song, T. Kakuta, T.-a. Yamagishi, Y.-W. Yang and T. Ogoshi, *Chem*, 2018, **4**, 2029–2053.
13 T. Ogoshi, S. Kanai, S. Fujinami, T.-a. Yamagishi and Y. J. Nakamoto, *J. Am. Chem. Soc.*, 2008, **130**, 5022–5023.
14 N. L. Strutt, H. Zhang, S. T. Schneebeli and J. F. Stoddart, *Acc. Chem. Res.*, 2014, **47**, 2631–2642.
15 T. Ogoshi, T. A. Yamagishi and Y. Nakamoto, *Chem. Rev.*, 2016, **116**, 7937–8002.
16 J.-R. Wu, A. U. Mu, B. Li, C.-Y. Wang, L. Fang and Y.-W. Yang, *Angew. Chem., Int. Ed.*, 2018, **57**, 9853.
17 D. Cao, Y. Kou, J. Liang, Z. Chen, L. Wang and H. Meier, *Angew. Chem., Int. Ed.*, 2009, **48**, 9721.
18 B. Yuan, J.-F. Xu, C.-L. Sun, H. Nicolas, M. Schönhoff, Q.-Z. Yang and X. Zhang, *ACS Appl. Mater. Interfaces*, 2016, **8**, 3679–3685.
19 L.-L. Tan, H. Li, Y. Tao, S.-X. Zhang, B. Wang and Y.-W. Yang, *Adv. Mater.*, 2014, **26**, 7027–7031.
20 L.-L. Tan, Y. Zhu, H. Long, Y. Jin, W. Zhang and Y.-W. Yang, *Chem. Commun.*, 2017, **53**, 6409–6412.
21 X. Li, Z. Li and Y.-W. Yang, *Adv. Mater.*, 2018, **30**, 1800177.
22 N. L. Strutt, D. Fairen-Jimenez, J. Iehl, M. B. Lalonde, R. Q. Snurr, O. K. Farha, J. T. Hupp and J. F. Stoddart, *J. Am. Chem. Soc.*, 2012, **134**, 17436–17439.
23 D. Dai, Z. Li, J. Yang, C. Wang, J.-R. Wu, Y. Wang, D. Zhang and Y.-W. Yang, *J. Am. Chem. Soc.*, 2019, **141**, 4756–4763.
24 J.-R. Wu, B. Li, J.-W. Zhang and Y.-W. Yang, *ACS Appl. Mater. Interfaces*, 2019, **11**, 998–1003.
25 J.-R. Wu and Y.-W. Yang, *J. Am. Chem. Soc.*, 2019, **141**, 12280–12287.
26 M.-X. Wu and Y.-W. Yang, *Polym. Chem.*, 2019, **10**, 2980–2985.
27 Y. Cui, B. Li, H. He, W. Zhou, B. Chen and G. Qian, *Acc. Chem. Res.*, 2016, **49**, 483–493.
28 B. Chen, Y. Yang, F. Zapata, G. Lin, G. Qian and E. B. Lobkovsky, *Adv. Mater.*, 2007, **19**, 1693–1696.
29 Y. Cui, H. Xu, Y. Yue, Z. Guo, J. Yu, Z. Chen, J. Gao, Y. Yang, G. Qian and B. Chen, *J. Am. Chem. Soc.*, 2012, **134**, 3979–3982.
30 O. M. Yaghi, G. M. Li and H. L. Li, *Nature*, 1995, **378**, 703–706.
31 H. Li, M. Eddaoudi, M. O'Keeffe and O. M. Yaghi, *Nature*, 1999, **402**, 276–279.
32 D. J. Lun, G. I. Waterhouse and S. G. Telfer, *J. Am. Chem. Soc.*, 2011, **133**, 5806–5809.
33 A. Mallick, A. M. El-Zohry, O. Shekhah, J. Yin, J. Jia, H. Aggarwal, A. H. Emwas, O. F. Mohammed and M. Eddaoudi, *J. Am. Chem. Soc.*, 2019, **141**, 7245–7249.
34 M. Eddaoudi, D. B. Moler, H. L. Li, B. L. Chen, T. M. Reineke, M. O'Keeffe and O. M. Yaghi, *Acc. Chem. Res.*, 2001, **34**, 319–330.
35 A. Cadiau, K. Adil, P. M. Bhatt, Y. Belmabkhout and M. Eddaoudi, *Science*, 2016, **353**, 137–140.
36 E. J. Carrington, C. A. McAnally, A. J. Fletcher, S. P. Thompson, M. Warren and L. Brammer, *Nat. Chem.*, 2017, **9**, 882–889.
37 L. Zhu, L. Zong, X. Wu, M. Li, H. Wang, J. You and C. Li, *ACS Nano*, 2018, **12**, 4462–4468.
38 Y. Xue, S. Zheng, H. Xue and H. Pang, *J. Mater. Chem. A*, 2019, **7**, 7301–7327.
39 X.-Y. Guo, F. Zhao, J.-J. Liu, Z.-L. Liu and Y.-Q. Wang, *J. Mater. Chem. A*, 2017, **5**, 20035–20043.
40 Y. Cui, Y. Yue, G. Qian and B. Chen, *Chem. Rev.*, 2012, **112**, 1126–1162.
41 Y. Liu, S.-Y. Moon, J. T. Hupp and O. K. Farha, *ACS Nano*, 2015, **9**, 12358–12364.
42 A. Cadiau, Y. Belmabkhout, K. Adil, P. M. Bhatt, R. S. Pillai, A. Shkurenko, C. Martineau-Corcos, G. Maurin and M. Eddaoudi, *Science*, 2017, **356**, 731–735.
43 B. W. Abbott, K. Bishop, J. P. Zarnetske, C. Minaudo, F. S. Chapin, S. Krause, D. M. Hannah, L. Conner, D. Ellison, S. E. Godsey, S. Plont, J. Marçais, T. Kolbe, A. Huebner, R. J. Frei, T. Hampton, S. Gu, M. Buhman, S. S. Sayedi, O. Ursache, M. Chapin, K. D. Henderson and G. Pinay, *Nat. Geosci.*, 2019, **12**, 533–540.
44 Y. Salinas, R. Martinez-Manez, M. D. Marcos, F. Sancenon, A. M. Costero, M. Parra and S. Gil, *Chem. Soc. Rev.*, 2012, **41**, 1261–1296.
45 S. Pramanik, C. Zheng, X. Zhang, T. J. Emge and J. Li, *J. Am. Chem. Soc.*, 2011, **133**, 4153–4155.
46 Z. Li, N. Song and Y.-W. Yang, *Matter*, 2019, **1**, 345–368.
47 X. Wang, Z.-J. Liu, E. H. Hill, Y. Zheng, G. Guo, Y. Wang, P. S. Weiss, J. Yu and Y.-W. Yang, *Matter*, 2019, **1**, 848–861.
48 X. Li, J. Han, X. Wang, Y. Zhang, C. Jia, J. Qin, C. Wang, J.-R. Wu, W. Fang and Y.-W. Yang, *Mater. Chem. Front.*, 2019, **3**, 103–110.
49 J.-N. Hao and B. Yan, *Adv. Funct. Mater.*, 2017, **27**, 1603856.
50 C. Krishnaraj, A. M. Kaczmarek, H. S. Jena, K. Leus, N. Chaoui, J. Schmidt, R. V. Deun and P. V. D. Voort, *ACS Appl. Mater. Interfaces*, 2019, **30**, 27343–27352.
51 G. Li, Z. Hou, C. Peng, W. Wang, Z. Cheng, C. Li, H. Lian and J. Lin, *Adv. Funct. Mater.*, 2010, **20**, 3446–3456.
52 Z. Li, G. Wang, Y. Wang and H. Li, *Angew. Chem., Int. Ed.*, 2018, **57**, 2194–2198.
53 T. Wang, P. Li and H. Li, *ACS Appl. Mater. Interfaces*, 2014, **6**, 12915–12921.
54 W. Zhou, Y. Chen, Q. Yu, P. Li, X. Chen and Y. Liu, *Chem. Sci.*, 2019, **10**, 3346–3352.
55 Y. Zhou, H.-Y. Zhang, Z.-Y. Zhang and Y. Liu, *J. Am. Chem. Soc.*, 2017, **139**, 7168–7171.
56 X. Zhao, B. Pattengale, D. Fan, Z. Zou, Y. Zhao, J. Du, J. Huang and C. Xu, *ACS Energy Lett.*, 2018, **3**, 2520–2526.
57 Y.-Q. Sun, J. Zhang, Z.-F. Ju and G.-Y. Yang, *Cryst. Growth Des.*, 2005, **5**, 1939–1943.
58 G. Fan, C. Feng and Z. Zhang, *J. Rare Earths*, 2007, **25**, 42–47.
59 X. Tan, Q. Fan, X. Wang and B. Grambow, *Environ. Sci. Technol.*, 2009, **43**, 3115–3121.
60 L. Shangguan, H. Xing, J. H. Mondal and B. Shi, *Chem. Commun.*, 2017, **53**, 889–892.
61 L. Shao, J. Sun, B. Hua and F. Huang, *Chem. Commun.*, 2018, **54**, 4866–4869.
62 J.-S. Ni, P. Zhang, T. Jiang, Y. Chen, H. Su, D. Wang, Z.-Q. Yu, R. T. K. Kwok, Z. Zhao, J. W. Y. Lam and B. Z. Tang, *Adv. Mater.*, 2018, **30**, 1805220.
63 J.-H. Wang, M. Li and D. Li, *Chem. Sci.*, 2013, **4**, 1793–1801.
64 B. Chen, Y. Yang, F. Zapata, G. Lin, G. Qian and E. B. Lobkovsky, *Adv. Mater.*, 2007, **19**, 1693–1696.